

Ultraviolet photoluminescence in Gd-doped silica and phosphosilicate fibers

Cite as: APL Photonics 2, 046101 (2017); <https://doi.org/10.1063/1.4976304>

Submitted: 23 October 2016 . Accepted: 31 January 2017 . Published Online: 17 February 2017

 Y. Wang, J. He, P. Barua, N. Chiodini, S. Steigenberger,  M. I. M. Abdul Khudus, J. K. Sahu, M. Beresna, and  G. Brambilla



View Online



Export Citation



CrossMark

ARTICLES YOU MAY BE INTERESTED IN

[Materials for optical fiber lasers: A review](#)

Applied Physics Reviews 5, 041301 (2018); <https://doi.org/10.1063/1.5048410>


[Electro-opto-mechanical radio-frequency oscillator driven by guided acoustic waves in standard single-mode fiber](#)

APL Photonics 2, 041303 (2017); <https://doi.org/10.1063/1.4977904>

[Wavelength conversion of QAM signals in a low loss CMOS compatible spiral waveguide](#)

APL Photonics 2, 046105 (2017); <https://doi.org/10.1063/1.4978945>

additive manufacturing epitaxial crystal growth cerium oxide polishing powder silver nanoparticles sputtering targets III-IV semiconductors CVD precursors europium phosphors

 AMERICAN ELEMENTS

THE ADVANCED MATERIALS MANUFACTURER®

deposition slugs OLED Lighting spintronics solar energy osmium nanoribbons thin films chalcogenides AuNPs GDC Li-ion battery electrolytes 99.999% ruthenium spheres

endohedral fullerenes copper nanoparticles diamond micropowder CIGS MBE grade materials palladium catalysts flexible electronics beta-barium borate borosilicate glass dysprosium pellets YBCO pyrolytic graphite 3d graphene foam indium tin oxide mesoporous silica raman substrates sapphire windows tungsten carbide InGaAs barium fluoride carbon nanotubes lithium niobate scandium powder

gallium lump glassy carbon nanodispersions InAs wafers laser crystals ultra high purity materials MOFs rare earth metals photovoltaics refractory metals MOCVD organometallics quantum dot superconductors transparent ceramics ultra high purity silicon

American Elements opens up a world of possibilities so you can **Now Invent!**

Over 15,000 certified high purity laboratory chemicals, metals, & advanced materials and a state-of-the-art Research Center. Printable GHS-compliant Safety Data Sheets. Thousands of new products. And much more. All on a secure multi-language "Mobile Responsive" platform.

perovskite crystals yttrium iron garnet alternative energy h-BN gold nanocubes graphene oxide macromolecules photonics rhodium sponge fiber optics beamsplitters infrared dyes zeolites fused quartz metallocenes platinum ink buckyballs Ti-6Al-4V

Now Invent.™
The Next Generation of Material Science Catalogs

www.americanelements.com



Ultraviolet photoluminescence in Gd-doped silica and phosphosilicate fibers

Y. Wang,^{1,a} J. He,¹ P. Barua,¹ N. Chiodini,² S. Steigenberger,³
 M. I. M. Abdul Khudus,^{1,4} J. K. Sahu,¹ M. Beresna,¹ and G. Brambilla¹

¹Optoelectronics Research Centre, University of Southampton, Southampton SO17 1BJ, United Kingdom

²Dipartimento di Scienza dei Materiali, Università di Milano Bicocca, 20126 Milan, Italy

³National Oceanography Centre, University of Southampton Waterfront Campus, European Way, Southampton SO14 3ZH, United Kingdom

⁴Photonics Research Centre, Department of Physics, Faculty of Science, University of Malaya, 50603 Kuala Lumpur, Malaysia

(Received 23 October 2016; accepted 31 January 2017; published online 17 February 2017)

Optical fiber lasers operating in the near infrared and visible spectral regions have relied on the spectroscopic properties of rare earth ions such as Yb³⁺, Er³⁺, Tm³⁺, Nd³⁺, and Sm³⁺. Here, we investigate Gd³⁺ doping in phosphosilicate and pure silica fibers using solution doping and sol-gel techniques, respectively, for potential applications in the ultraviolet. Photoluminescence spectra for optical fiber bundles and fiber preforms were recorded and compared. Emissions at 312 nm (phosphosilicate) and 314 nm (pure silica) were observed when pumping to the Gd³⁺ ⁶D_J, ⁶I_J, and ⁶P_{J=5/2, 3/2} energy levels. Oxygen deficient center was observed in solution doping sample with a wide absorption band centered at around 248 nm not affecting pumping to ⁶I_J states. © 2017 Author(s). All article content, except where otherwise noted, is licensed under a Creative Commons Attribution (CC BY) license (<http://creativecommons.org/licenses/by/4.0/>). [<http://dx.doi.org/10.1063/1.4976304>]

Ultraviolet (UV) light sources have found numerous applications in medical science and engineering, such as disinfection, water purification, food manufacturing, UV curing, and lithography,^{1–4} as short wavelengths have relatively high photon energy and provide high resolution. Currently, UV sources consist mostly of gas lasers,⁵ lamps, or diodes¹ or rely on nonlinear optical processes, such as third/fourth harmonic generation or optical parametric oscillators (OPOs).^{6,7} Fiberized laser sources could be an attractive alternative to conventional UV sources. Fiber based light sources exhibit excellent beam quality, extraordinary brightness, small detrimental thermal effects, and high temporal stability. Fiber lasers operating in the near infrared (IR) and visible mostly rely on the spectroscopic properties of rare earth ions.⁸ High-power Yb³⁺-doped fiber lasers at the wavelength of $\lambda \sim 1 \mu\text{m}$ have found extensive applications in metal processing like welding, milling, and marking.^{9,10} Extension to the UV would benefit applications such as precise micromachining and processing/marking of insulators, which are usually energy inefficient when carried out with near IR lasers and would benefit from an improved optical absorption, higher resolution as well as minimized thermal damage.

Gd³⁺ has its first excited state located at a wavenumber $\tilde{\nu} \sim 32\,000 \text{ cm}^{-1}$ above the ground level (Fig. 1(a)), corresponding to an UV emission at $\lambda \sim 312.5 \text{ nm}$. Simultaneously, silica glass, the host material, has various advantages including transparency in the UV down to $\lambda \sim 200 \text{ nm}$,^{11,12} extraordinary mechanical strength, strong chemical and radiation resistance, and compatibility with existing silica-based components. The silica network has a high phonon energy ($\tilde{\nu} \sim 1100 \text{ cm}^{-1}$); therefore, transitions among the ⁶D_J, ⁶I_J and ⁶P_J energy levels in Gd³⁺-doped silica tend to be dominated by non-radiative multi-phonon relaxation due to the small energy gaps. Previous studies of Gd-doped samples in film, bulk, and powder form under electron-beam, vacuum ultraviolet (VUV), and X-ray excitation^{13–15} suggest that the emission at $\lambda \sim 312 \text{ nm}$, given by the ⁶P_{7/2} → ⁸S_{7/2} transition,

^aAuthor to whom correspondence should be addressed. Electronic mail: yw11e13@soton.ac.uk.



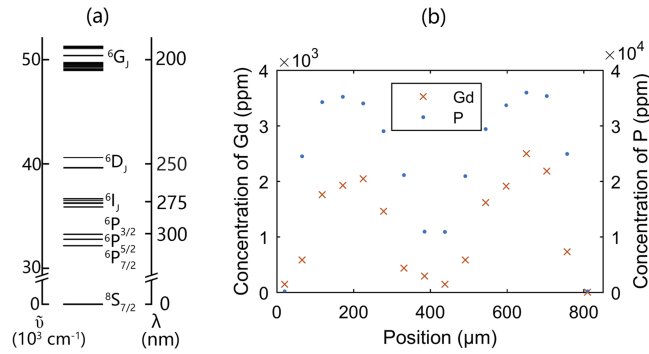


FIG. 1. (a) Gd³⁺ energy levels with wavenumbers ($\tilde{\nu}$) and wavelengths (λ) of the photons emitted in the transition to the ground level (adapted from Refs. 19 and 20). (b) EDX scan of the Gd³⁺-doped phosphosilicate preform core area. The dip at the preform center is commonly observed in MCVD fiber preforms and is attributed to the evaporation of P₂O₅ during consolidation, which also removed Gd³⁺.

would be a promising candidate for the generation of light in the UV. The lifetime of the $^6P_{7/2}$ level has been found to be 5 ms in a sol-gel sample containing ~ 3 mol. % of Gd.¹⁶ Rapid thermal treatment on Gd-doped sol-gel silica bulk sample resulted in an enhancement in Gd³⁺ luminescence.¹⁷ This work investigates the luminescence of Gd³⁺ in silica fibers as a possible candidate for the development of coherent solid state sources in the UV.

Two types of Gd³⁺-doped fiber samples with a pure silica and a phosphosilicate core were studied. The phosphosilicate sample was fabricated using the modified chemical vapor deposition (MCVD) and solution doping techniques.¹⁸ The core layer, formed by un-sintered porous soot, was deposited inside a silica tube (F-300, Heraeus) at a temperature $T \sim 1530$ °C by oxidizing the vapor-phase precursors SiCl₄ and POCl₃. The tube was subsequently soaked for about 1 h in a solution containing GdCl₃·6H₂O dissolved in methanol. The core layer was then sintered and the tube was collapsed into a preform with a silica cladding and a Gd³⁺-doped phosphosilicate core. The dopant concentration along the preform core cross section was measured by energy-dispersive X-ray (EDX) spectroscopy in a sample cut from the fiber preform (Fig. 1(b)). The Gd³⁺ concentration reaches its maximum, >2000 ppm by mol, at a position 200 μm away from the preform center. The decreased concentration level at the preform center was attributed to the evaporation of P₂O₅ during the consolidation process, which also removed Gd³⁺. The average atomic percentage of Gd³⁺ across the preform core cross section was determined as ~ 1170 ppm by mol. The preform was subsequently pulled into an optical fiber at a temperature $T \sim 2040$ °C. The fiber had core and cladding diameters of $d_{\text{co}} = 5.8$ μm and $d_{\text{cl}} = 125$ μm , respectively, and a numerical aperture (NA) of 0.13.

A second fiber was manufactured using the rod-in-tube technique with a fluorosilicate cladding and a silica rod doped with 1000 ppm molar Gd fabricated via sol-gel.²¹ Tetramethoxysilane (TMOS) and Gd³⁺ nitrate were put under sol-gel reaction in a methanol:water 4:1 solution. After gelation at $T \sim 45$ °C, the alcogel was subsequently slowly dried to a xerogel in a thermostatic chamber at the same temperature, and finally densified under controlled atmosphere in a suitable oven at $T \sim 1250$ °C and a further final densification was achieved during a fiber drawing process at a temperature above $T \sim 2000$ °C. The Gd-doped sample was pulled into a 500 μm diameter cane.

The transmission spectrum of a 15 cm-long phosphosilicate fiber sample (Fig. 2(a)) shows dips at $\lambda \sim 244.8$ nm, 247.1 nm, 253.2 nm, 273.4–274.6 nm, 276.4 nm, 279.4 nm, 301.4 nm, 306.3 nm, and 311.9 nm, which were attributed to the Gd³⁺ transitions from the fundamental ($^8S_{7/2}$) to the 6D_1 , 6I_1 , 6P_1 levels and are in agreement with the energy levels reported in the literature^{19,20} and summarized in Fig. 1(a). The spectrum was collected using a broadband deuterium lamp source (BDS130, BWTEK), a spectrometer (USB4000, Ocean Optics) equipped with a 25 μm slit, and a UV transparent fiber for the reference spectrum and power delivery into the sample. Although the host material of the data reported in the literature is different, it is well known that in rare earth ions the 4f electronic states are screened by the outer 5s² and 5p⁶ electron shells, thus the positions of the absorption and emission spectral lines are weakly affected by the host environment. The propagation losses at 309 nm

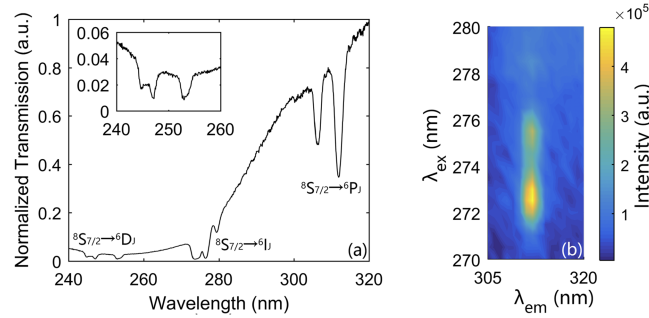


FIG. 2. (a) Phosphosilicate fiber transmission spectrum. (b) 2D PL/PLE spectral mapping of the phosphosilicate fiber sample. The excitation and emission mapping step were 0.5 nm and 1 nm, respectively.

and 317 nm, measured using the cut back method, were estimated to be ~ 1.8 dB/m and ~ 1.3 dB/m, respectively. The weaker output at short wavelengths in Fig. 2(a) was mostly attributed to the absorption associated with defects²² and the bandgap of phosphosilicate glass²³ which can be further optimized. The broad absorption peak centered at $\lambda \sim 250$ nm has been attributed to oxygen deficient centers (ODCs) and impeded the loss characterization of the Gd^{3+} transitions from the ground levels to the ${}^6\text{D}_j$ and ${}^6\text{I}_j$ via cut back method.

2D photoluminescence (PL) and photoluminescence excitation (PLE) spectral mapping of the phosphosilicate fiber sample (Fig. 2(b)) were recorded at room temperature with a Horiba Fluorolog-3 spectrofluorometer equipped with a xenon excitation lamp and corrected for excitation spectrum, detector spectral sensitivity, and blaze angle of emission grating. In order to improve the signal to noise ratio (SNR) and obtain a significant signal from the fiber sample, a bundle of approximately 10^3 fibers without polymer coating was assembled to form a parallelepiped with dimensions $1 \text{ cm} \times 1 \text{ cm} \times 1 \text{ mm}$ (Fig. 3(a)). Light was incident on the fiber side, which has the highest core to cladding aspect ratio. Both the excitation and emission slits were set to 1 nm bandpass with an estimated beam size of $1 \text{ mm} \times 6.5 \text{ mm}$ at the sample surface. In the spectral mapping, intense PL emission at $\lambda_{\text{em}} \sim 312$ nm, given by the ${}^6\text{P}_{7/2} \rightarrow {}^8\text{S}_{7/2}$ transition, was observed under excitation at $\lambda_{\text{ex}} = 272.7$ nm and 275.4 nm, i.e., pumping into the Gd^{3+} ${}^6\text{I}_j$ multiplet levels. A ~ 1 nm shift from the absorption spectrum was attributed to the different calibrations of the spectrometer and the spectrofluorometer used.

As the fiber drawing process corresponds to a thermal treatment at high temperature, fiber preforms were also analyzed for comparisons. A disk was cut from the phosphosilicate preform with a core diameter of 0.8 mm and its cross section polished to minimize scattering (Fig. 3(b)). Disks cut from sol-gel silica samples without any cladding layer have been studied in Ref. 24.

The phosphosilicate preform disk exhibits intense emissions at $\lambda_{\text{em}} = 311.7$ nm, attributed to the Gd^{3+} ${}^6\text{P}_{7/2} \rightarrow {}^8\text{S}_{7/2}$ transition, observed under excitations at $\lambda_{\text{ex}} = 243.7$ nm, 245.7 nm, and 251.9 nm, attributed to pumping into the ${}^6\text{D}_j$ levels; excitations at $\lambda_{\text{ex}} = 272.6$ nm, 275.2 nm, and 278.3 nm, attributed to pumping into the ${}^6\text{I}_j$ levels; and excitations at $\lambda_{\text{ex}} = 304.0$ nm, attributed to pumping into the ${}^6\text{P}_{5/2}$ levels, respectively (Fig. 4). A comparison with the results obtained for the fiber sample (Fig. 2(b)) suggests that the emission wavelengths, thus the energy levels of the Gd^{3+} dopant, were

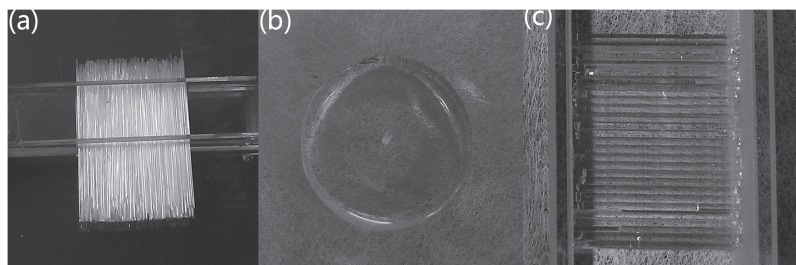


FIG. 3. (a) Phosphosilicate fiber bundle, (b) phosphosilicate preform disk, and (c) silica fiber bundle hold in a cuvette.

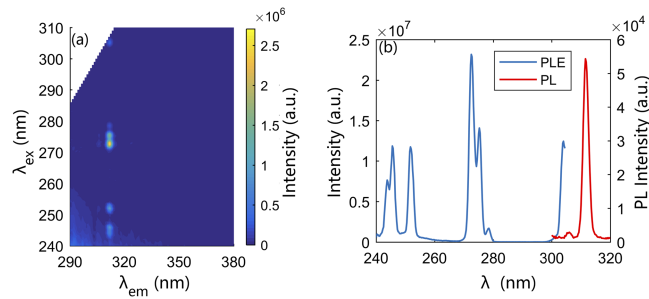


FIG. 4. (a) 2D PL/PLE spectral mapping of the phosphosilicate preform disk. Due to the weak excitation intensity at short wavelengths, mappings were taken on multiple sub-areas with scanning step ranging from 0.5 nm to 2 nm before combination. (b) PL (excitation wavelength $\lambda_{\text{ex}} = 272.5$ nm) and PLE (emission wavelength $\lambda_{\text{em}} = 312$ nm) spectra. Slit widths as well as the peak values differ because of the increased excitation and emission slit widths used for PL and PLE signal optimizations, respectively. The wavelength ranges are limited to the data available for correction, based on the wavelength dependent source power and detector sensitivity.

unaffected by the fiber pulling process performed at high temperature. The ${}^6\text{P}_{7/2} \rightarrow {}^8\text{S}_{7/2}$ transition, which features a spin change, is associated with an emission band having a linewidth of $\Delta\lambda \sim 2.5$ nm (FWHM). The relatively strong emission signal at excitation of $\lambda_{\text{ex}} = 272.5$ nm is partly attributed to the dense distribution of energy levels in the ${}^6\text{I}_j$ energy level group (Fig. 1(a)) which results in multiple lines broadened by glass host and overlapping within the bandpass 1 nm wavelength range. At this excitation, a weak emission from the ${}^6\text{P}_{5/2}$ energy level was also observed at $\lambda_{\text{em}} \sim 306$ nm in the PL spectrum. Excitation to this level, followed by an inter-band non-radiative decay to ${}^6\text{P}_{7/2}$, corresponds to a peak at $\lambda_{\text{em}} \sim 304$ nm in the PLE spectrum, suggesting a Stokes shift of $\Delta\lambda \sim 2$ nm.

The polished disk sample (Fig. 4(a)) showed a higher SNR than the fiber bundle (Fig. 2(b)). Although the SNR is relatively low at short excitation wavelengths mostly due to the weak intensity of the light source below $\lambda_{\text{ex}} \sim 250$ nm, a weak signal from ODC(II)²⁵ was clearly observed as a wide-band emission (see the left bottom of Fig. 4(a)). Despite of the wide transparency range of pure silica, various types of defects can induce loss in the UV wavelength region. ODC is one of the most common silica defects optically active in the UV region and has attracted particular interest due to its photoluminescence features.²⁵ The excitation spectra for two characteristic emission wavelengths of the ODC(II), namely, $\lambda_{\text{em}} \sim 282$ nm and $\lambda_{\text{em}} \sim 459$ nm,²⁶ were verified (Fig. 5). Its absorption band overlaps with some of the transitions in Gd^{3+} , thus it would affect the pump efficiency in potential applications.

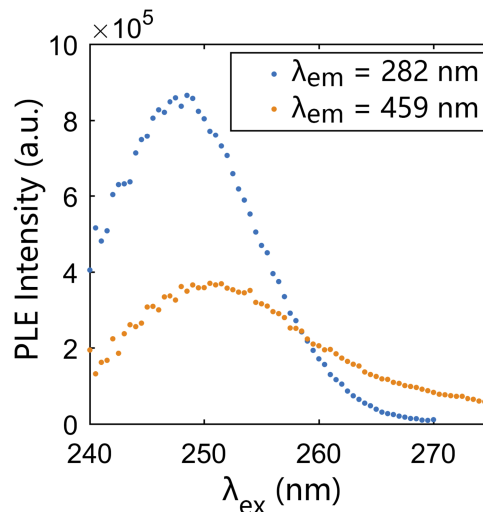


FIG. 5. PLE spectra of ODCs at two emission wavelengths (λ_{em}) in the phosphosilicate preform sample.

The PL/PLE mapping and PL(E) spectra from the Gd^{3+} -doped silica fiber sample were recorded with a wavelength step of 0.5 nm and slit widths of 1 nm (Fig. 6). A stack of fifty Gd^{3+} -doped silica fiber canes without polymer coating was prepared to form a parallelepiped with dimensions 1 cm \times 1 cm \times 1 mm. Results showed an approximately $\Delta\lambda \sim 1.5$ nm shift in the Gd^{3+} emission wavelengths with respect to the phosphosilicate sample. A weak luminescence signal at $\lambda_{\text{em}} \sim 325$ nm, nearly $\Delta\tilde{\nu} \sim 1100$ cm^{-1} from $\lambda_{\text{em}} \sim 314$ nm, matches the Raman shift associated to the Si–O–Si fundamental vibration. Compared with the phosphosilicate sample, instead of the ODC(II) emission band, a wide-band emission at $\lambda_{\text{em}} \sim 390$ nm previously observed in the disk sample²⁴ was detected here but with its peak intensity reduced to about 1/18 of the peak PL intensity from Gd^{3+} . This wavelength is close to the $T_1 \rightarrow S_0$ transition of the Ge-ODC²⁷ which was previously detected in silica containing germanium (Ge) impurities at concentrations of the order of 10 ppm by weight.²⁸ In this preform, Ge might have been induced during preform fabrication using the sol-gel method in the form of impurity in the silicon precursors. However, here the excitation-wavelength-dependent peak position implies a more complex explanation. Since this signal was not observed in the phosphosilicate samples, it is currently supposed to emerge from intrinsic defects of the host. The difference in intensity between Gd^{3+} luminescence and this signal increased in comparison to that recorded in the sol-gel disk sample before the fiber drawing process.²⁴ As the fiber pulling process corresponds to a rapid thermal treatment of the sample, this phenomenon is in accordance with the enhanced Gd luminescence observed in the literature after rapid thermal treatment.¹⁷ Besides, the excitation peak at $\lambda_{\text{ex}} = 307.5$ nm (to ${}^6P_{5/2}$ level) features a shoulder at 305.5 nm, which is different from the peak profile observed previously. This difference is similar to the host-dependent $\text{Er}^{3+} {}^4I_{13/2} \rightarrow {}^4I_{15/2}$ transition.⁸ Both phenomena confirmed that the Gd^{3+} experience a different surrounding in the silica and phosphosilicate samples.²⁹ Further analysis on the emission at $\lambda_{\text{em}} \sim 390$ nm will be carried out in the future.

In conclusion, PL and PLE spectra before and after fiber drawing show that phosphosilicate and pure silica fibers doped with Gd^{3+} are optically active in the UV with emissions observed at $\lambda_{\text{em}} \sim 312$ and 314 nm when the samples are pumped at $\lambda_{\text{ex}} \sim 272.5$ nm or 252 nm in the phosphosilicate sample and $\lambda_{\text{em}} \sim 274$ nm or 253 nm in the silica sample, respectively.

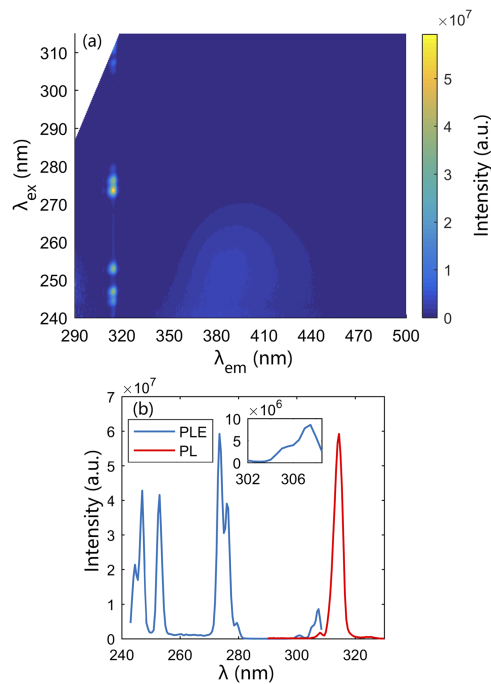


FIG. 6. (a) 2D PL/PLE spectral mapping, (b) PL ($\lambda_{\text{ex}} = 274$ nm) and PLE ($\lambda_{\text{em}} = 314$ nm) spectra of the Gd^{3+} -doped silica fiber sample extracted from 2D mapping.

The authors gratefully acknowledge support from Engineering and Physical Sciences Research Council (No. EP/L01243X/1). All data supporting this study are openly available from the University of Southampton repository at <http://doi.org/10.5258/SOTON/402084>.

- ¹ K. Song, M. Mohseni, and F. Taghipour, *Water Res.* **94**, 341 (2016).
- ² T. Bintsis, E. Litopoulou-Tzanetaki, and R. K. Robinson, *J. Sci. Food Agric.* **80**, 637 (2000).
- ³ A. Endruweit, M. S. Johnson, and A. C. Long, *Polym. Compos.* **27**, 119 (2006).
- ⁴ M. Han, W. Lee, S.-K. Lee, and S. S. Lee, *Sens. Actuators A* **111**, 14 (2004).
- ⁵ J. M. Hoffman, A. K. Hays, and G. C. Tisone, *Appl. Phys. Lett.* **28**, 538 (1976).
- ⁶ H. M. Pask, P. Dekker, R. P. Mildren, D. J. Spence, and J. A. Piper, *Prog. Quantum Electron.* **32**, 121 (2008).
- ⁷ G. K. Samanta, S. C. Kumar, A. Aadhi, and M. Ebrahim-Zadeh, *Opt. Express* **22**, 11476 (2014).
- ⁸ W. Miniscalco, in *Rare-Earth-Doped Fiber Lasers Amplifiers*, 2nd ed. Revised Expand, edited by M. J. F. Digonnet (CRC Press, New York, 2001).
- ⁹ E. Williams, E. B. Brousseau, and A. Rees, *Int. J. Adv. Manuf. Technol.* **74**, 769 (2014).
- ¹⁰ J. Gabzdyl, *Nat. Photonics* **2**, 21 (2008).
- ¹¹ G. Siegel, *J. Non-Cryst. Solids* **13**, 372 (1974).
- ¹² See <https://www.fiberguide.com/wp-content/uploads/2012/09/Solarguide.090712.pdf> for attenuation spectrum of commercialized UV fiber from Fiberguide Company, Stirling, New Jersey, accessed 11 October 2016.
- ¹³ U. Vetter, J. Zenneck, and H. Hofsäss, *Appl. Phys. Lett.* **83**, 2145 (2003).
- ¹⁴ Z. Yang, J. Lin, M. Su, Y. Tao, and W. Wang, *J. Alloys Compd.* **308**, 94 (2000).
- ¹⁵ Z. Tian, H. Liang, B. Han, Q. Su, Y. Tao, G. Zhang, and Y. Fu, *J. Phys. Chem. C* **112**, 12524 (2008).
- ¹⁶ N. Chiodini, M. Fasoli, M. Martini, F. Morazzoni, E. Rosetta, R. Scotti, G. Spinolo, A. Vedda, M. Nikl, N. Solovieva, A. Baraldi, R. Capelletti, and R. Francini, *Radiat. Eff. Defects Solids* **158**, 463 (2003).
- ¹⁷ D. Di Martino, N. Chiodini, M. Fasoli, F. Moretti, A. Vedda, A. Baraldi, E. Buffagni, R. Capelletti, M. Mazzer, M. Nikl, G. Angella, and C. B. Azzoni, *J. Non-Cryst. Solids* **354**, 3817 (2008).
- ¹⁸ J. E. Townsend, S. B. Poole, and D. N. Payne, *Electron. Lett.* **23**, 329 (1987).
- ¹⁹ G. H. Dieke and H. M. Crosswhite, *Appl. Opt.* **2**, 675 (1963).
- ²⁰ R. T. Wegh, A. Meijerink, R.-J. Lamminmäki, and J. Hölsä, *J. Lumin.* **87-89**, 1002 (2000).
- ²¹ F. Moretti, N. Chiodini, M. Fasoli, L. Griguta, and A. Vedda, *J. Lumin.* **126**, 759 (2007).
- ²² H. Imai, K. Arai, H. Imagawa, H. Hosono, and Y. Abe, *Phys. Rev. B* **38**, 12772 (1988).
- ²³ M. Engholm and L. Norin, *Opt. Express* **16**, 1260 (2008).
- ²⁴ J. He, Y. Wang, S. Steigenberger, A. Macpherson, N. Chiodini, and G. Brambilla, in *Conference on Lasers Electro-Optics* (OSA, Washington, DC, 2016), p. JTh2A.86.
- ²⁵ R. Salh, *Crystalline Silicon-Properties and Uses*, edited by S. Basu (InTech, 2011), pp. 135–172.
- ²⁶ L. Skuja, *J. Non-Cryst. Solids* **239**, 16 (1998).
- ²⁷ G. Pacchioni, L. Skuja, and D. L. Griscom, *Defects in SiO₂ and Related Dielectrics: Science and Technology* (Springer Netherlands, Dordrecht, Netherlands, 2000), p. 314.
- ²⁸ M. Cannas, in *GNSR 2001 State Art Futur: Dev. Raman Spectrosc. Relat. Tech.*, edited by G. Messina and S. Santangelo (IOS Press, 2002), pp. 91–112.
- ²⁹ A. Saitoh, S. Matsuishi, C. Se-Weon, J. Nishii, M. Oto, M. Hirano, and H. Hosono, *J. Phys. Chem. B* **110**, 7617 (2006).